



## Drug Design Hot Paper

How to cite: *Angew. Chem. Int. Ed.* **2022**, *61*, e202204052

International Edition: doi.org/10.1002/anie.202204052

German Edition: doi.org/10.1002/ange.202204052

# Rational Design of a Novel Tubulin Inhibitor with a Unique Mechanism of Action

Tobias Mühlethaler<sup>†</sup>, Lampros Milanos<sup>†,\*</sup>, Jose Antonio Ortega, Thorsten B. Blum, Dario Gioia, Bibhas Roy, Andrea E. Prota, Andrea Cavalli,<sup>\*</sup> and Michel O. Steinmetz<sup>\*</sup>

**Abstract:** In this study, we capitalized on our previously performed crystallographic fragment screen and developed the antitubulin small molecule Todalam with only two rounds of straightforward chemical synthesis. Todalam binds to a novel tubulin site, disrupts microtubule networks in cells, arrests cells in G2/M, induces cell death, and synergizes with vinblastine. The compound destabilizes microtubules by acting as a molecular plug that sterically inhibits the curved-to-straight conformational switch in the  $\alpha$ -tubulin subunit, and by sequestering tubulin dimers into assembly incompetent oligomers. Our results describe for the first time the generation of a fully rationally designed small molecule tubulin inhibitor from a fragment, which displays a unique molecular mechanism of action. They thus demonstrate the usefulness of tubulin-binding fragments as valuable starting points for innovative antitubulin drug and chemical probe discovery campaigns.

## Introduction

Microtubules are cytoskeletal filaments that are assembled from and disassembled into their  $\alpha\beta$ -tubulin heterodimeric building blocks. Because microtubules are implicated in several important cellular activities, including cell division, cell motility, and intracellular trafficking, drugs that interfere with microtubule functions have been developed very successfully as chemotherapeutics to fight against different

malignant tumors (reviewed in Ref. [1]). A significant breakthrough was achieved when paclitaxel (Taxol<sup>®</sup>) became the first-line blockbuster drug for the treatment of ovarian, breast, bladder, prostate, and lung cancers. Since then, several additional antitubulin drugs were introduced in the clinic, including epothilone (Ixempra<sup>®</sup>) and eribulin (Halaven<sup>®</sup>). However, despite massive medical successes, their wider application is hampered by toxicity and the development of resistance.<sup>[2]</sup> Furthermore, since antitubulin drugs are typically derived from natural products, their chemical structures are complex and thus difficult and expensive to produce synthetically in high quantities.

Several dozen different chemical classes of antitubulin agents are known today. They can be broadly divided into microtubule-stabilizing and microtubule-destabilizing agents. By interfering with microtubule dynamics during cell division, they arrest cells in mitosis and often promote senescence or apoptotic cell death, which is the primary strategy of chemotherapies. However, agents stabilizing microtubules have also been reported to be useful tools to restore damaged neurons<sup>[3]</sup> (reviewed in Ref. [4]). Furthermore, microtubules are considered promising targets for the development of new drugs against parasites and fungi<sup>[5]</sup> (reviewed in Ref. [6]). Antitubulin agents thus hold the promise that besides being still useful as next generation of chemotherapeutics (see Ref. [7] for candidates currently undergoing clinical trials), they could also be exploited to treat injuries and diseases of the nervous system or to combat infectious diseases.

Recent advances in the high-resolution structural analysis of tubulin and microtubules by X-ray crystallography and cryo-electron microscopy, respectively, made it possible to decipher the molecular mechanism of action of dozens of different antitubulin agents. In this context, seven different binding sites in the  $\alpha\beta$ -tubulin heterodimer were discovered.<sup>[8,9]</sup> Recently, using a very well-established tubu-

[\*] T. Mühlethaler,<sup>†</sup> T. B. Blum, A. E. Prota, M. O. Steinmetz  
 Laboratory of Biomolecular Research, Department of Biology and Chemistry, Paul Scherrer Institut  
 5232 Villigen PSI (Switzerland)  
 E-mail: michel.steinmetz@psi.ch

L. Milanos,<sup>†</sup> J. A. Ortega, D. Gioia, A. Cavalli  
 Computational & Chemical Biology, Istituto Italiano di Tecnologia  
 via Morego 30, 16163 Genova (Italy)  
 E-mail: lampros.milanosi@crl.com  
 andrea.cavalli@iit.it

B. Roy  
 Laboratory of Nanoscale Biology, Department of Biology and Chemistry, Paul Scherrer Institut  
 5232 Villigen PSI (Switzerland)

A. Cavalli  
 Department of Pharmacy and Biotechnology,  
 Alma Mater Studiorum, University of Bologna  
 via Belmeloro 6, 40126 Bologna (Italy)

M. O. Steinmetz  
 University of Basel, Biozentrum  
 4056 Basel (Switzerland)

[<sup>†</sup>] These authors contributed equally to this work.

© 2022 The Authors. Angewandte Chemie International Edition published by Wiley-VCH GmbH. This is an open access article under the terms of the Creative Commons Attribution Non-Commercial NoDerivs License, which permits use and distribution in any medium, provided the original work is properly cited, the use is non-commercial and no modifications or adaptations are made.

lin crystallization system,<sup>[10]</sup> we reported a crystallographic fragment screening study that allowed us to identify 56 chemically diverse fragments that target ten distinct tubulin sites.<sup>[11]</sup>

Here, we sought to test whether our identified fragments can be used as favorable starting points for the rapid generation of synthetic antitubulin, lead-like small molecules. To this end, we selected three distinct fragments that bind to a novel site on tubulin. Using a combined structural biology, computational, chemistry, biochemistry, and cell biology approach, we then developed the small molecule Todalam. Our results demonstrate that Todalam acts as a microtubule-destabilizing agent both in vitro and in cells via a unique molecular mechanism of action.

## Results and Discussion

### Fragment Selection

As a first step for our rational antitubulin-ligand design effort, we analyzed all binding sites and fragments revealed by our previously performed crystallographic fragment screen.<sup>[11]</sup> Among them, fragment site sID  $\beta$ II, which is located between two longitudinally aligned  $\alpha\beta$ -tubulin heterodimers (Figure 1A), captured our attention as it has not been described before. It is formed by residues of helices  $\beta$ H3',  $\beta$ H11', and  $\alpha$ H8, strand  $\alpha$ S4, and loops  $\beta$ T3,  $\beta$ T5,  $\alpha$ H3-S4, and  $\alpha$ H4- $\alpha$ S5 (Figure 1B; see Ref. [12] for designation of secondary structure elements and residue numbering). 16 fragments targeted site sID  $\beta$ II of which five contain an acetanilide group as a common binding motif (Figure S1). We selected fragment F04 (Figure 1C) to proceed with our ligand optimization strategy for the following reasons: (i) F04 displays the most molecular interactions within the binding site compared to the other fragments; (ii) we anticipated that several F04 derivatives could be produced in high quantities using mainly a well-established, one-step Hantzsch aminothiazole synthesis; (iii) F04 exhibits the highest molecular weight among all fragments and thus had the potential to be developed into a lead-like molecule after small modifications.

The tubulin-F04 crystal structure (PDB ID 5S4O) revealed that its acetanilide and thiazoleamine groups form three hydrogen bonds with the side chains of  $\beta$ N102,  $\alpha$ T257, and  $\beta$ K105 (water mediated), and one hydrogen bond with the side chain of  $\alpha$ Q133, respectively (Figure 1D; Figure S2A). In addition, the core phenyl moiety of the fragment establishes a  $\pi$ -stacking interaction with the side chain of  $\beta$ W407. This network of interactions causes the thiazoleamine group of the fragment to point towards a prominent, deep hydrophobic cavity in the  $\alpha$ -tubulin monomer. It is shaped by residues  $\alpha$ C4,  $\alpha$ F135,  $\alpha$ L136,  $\alpha$ L167,  $\alpha$ L242, and  $\alpha$ L252, and is occupied by three structural water molecules that establish hydrogen bonds amongst themselves and with the main and side chains of residues  $\alpha$ F135 and  $\alpha$ S165, respectively (Figure 1D; Figure S2A). Interestingly, the phenyl moieties of fragments F36 and F41 bound to this hydrophobic pocket and by doing so displaced the three

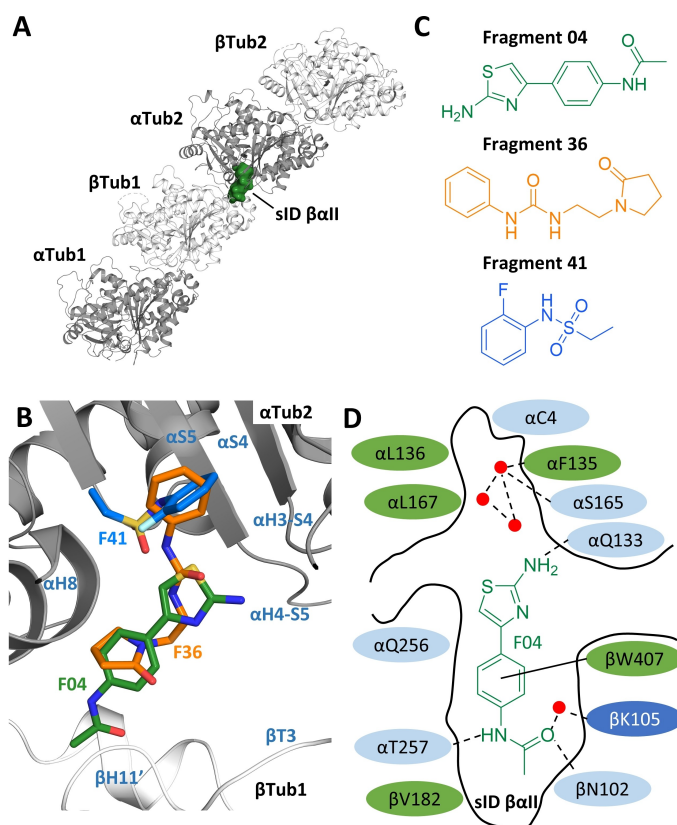


**Figure 1.** Fragment selection. A) Location of the site sID  $\beta$ II (volume representation) at the  $\beta$ Tub1- $\alpha$ Tub2 interdimer interface of the  $T_2$ R-TTL complex. For simplicity, the RB3 and TTL chains are not shown. The two  $\alpha$ - and two  $\beta$ -tubulin monomers in the  $T_2$ R-TTL complex are shown in grey and white ribbon representation, respectively. B) Superimposition of the F04, F36, and F41 binding poses (PDB IDs 5S4O, 5S5K, and 5S5P, respectively). Secondary structure elements of tubulin are labeled in blue. Carbon atoms are colored in green for F04, orange for fragment F36, and light blue for fragment F41. Nitrogen atoms are colored in blue, oxygen atoms in red, sulfur atoms in yellow, and fluorine atoms in light green. C) Chemical structures of fragments F04, F36, and F41. D) Schematic representation of F04 bound to site sID  $\beta$ II. Residues forming the binding site are shown in green for hydrophobic, in light blue for polar, and in dark blue for charged residues. The interacting residues  $\alpha$ L242 and  $\alpha$ L252 are not shown because they are located below the ligand. Hydrogen bonds are indicated with dashed and  $\pi$ -stacking interactions with solid black lines. Red dots represent crystallographic water molecules.

structural water molecules (Figure S2BC; PDB IDs 5S5K and 5S5P). This observation suggests that adding a phenyl substituent to the amino group linked to the thiazole heterocycle of F04 should be beneficial for gaining activity.

Notably, F04 also binds to a second site on  $\beta$ -tubulin, site sID  $\beta$ III, formed by residues of helix  $\beta$ H1', the N-terminus of  $\beta$ -tubulin, and loop  $\beta$ T7 (Figure S3A–C). Compared to site sID  $\beta$ II, the acetanilide group of F04 is solvent exposed and not well anchored in site sID  $\beta$ III, whereas its thiazoleamine moiety interacts with main chain atoms of residues of the  $\beta$ T7-loop. The amine group of the thiazoleamine forms a hydrogen bond with the main chain of  $\beta$ A250 and fills the space available between the  $\beta$ N-terminus and the  $\beta$ T7-loop (Figure S3B). We thus anticipated that even small modifica-

tions at this position should inhibit the binding of F04 to the alternative site sID  $\beta$ III.

### Synthesis of F04 Derivatives

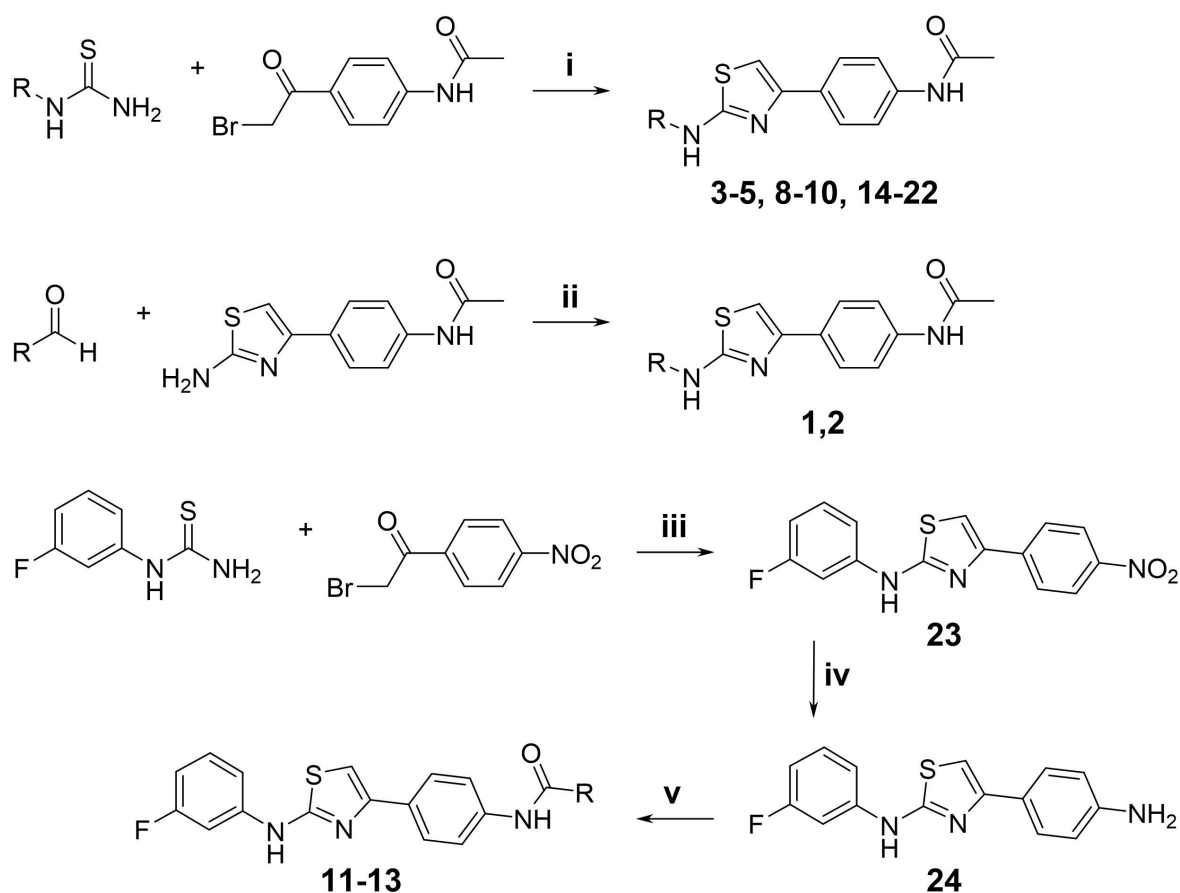
To confirm the structural observations and depict robust SARs, three different synthetic strategies were conceived to obtain F04 derivatives: Hantzsch synthesis, reductive amination, and acylation (Scheme 1). Most of the derivatives were obtained through Hantzsch reaction to form the thiazole core heterocycle. 4-Acetamidophenacyl bromide reacted with corresponding thioureas in ethanol at reflux temperature for 1 hour to yield compounds **3–5**, **8–10**, and **14–22** (Scheme 1) with moderate to good yields. Alkyl derivatives **1** and **2** were obtained under reductive amination conditions of N-(4-(2-aminothiazol-4-yl)phenyl)acetamide with isobutyraldehyde and trimethylacetaldehyde, respectively. Amide derivatives **11–13** were prepared in three steps. Firstly, the thiazole containing intermediate **23** was obtained through Hantzsch reaction conditions between 2-bromo-1-(4-nitrophenyl)ethanone and N-(3-fluorophenyl)thiourea with a good yield. Subsequently, the nitro group present in **23**

was reduced in presence of HCl and iron with moderate yields to get the amino intermediate **24** that finally was converted into amides **11–13** by reacting with corresponding acyl chlorides in the presence of the non-nucleophilic base DIPEA with moderate to good yields.

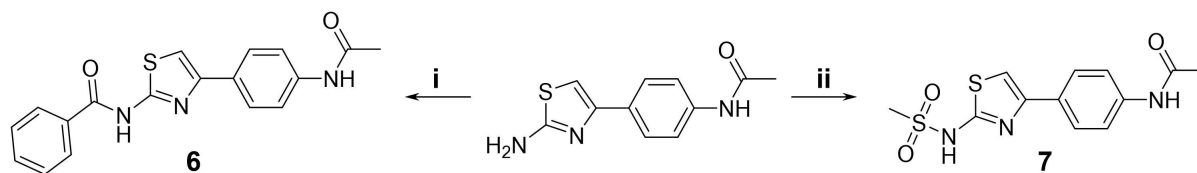
Compounds **6** and **7** were obtained from the common starting material N-(4-(2-aminothiazol-4-yl)phenyl)acetamide in one step with different synthetic approaches (Scheme 2). Compound **6** was synthesized by acylation with benzoylchloride in the presence of the non-nucleophilic base triethylamine with moderate yields, while sulphonamide derivative **7** was obtained by reaction with methanesulfonyl chloride in presence of pyridine as a base with good yields (Scheme 2).

### Fragment Linking

Using a standard cellular cytotoxicity assay, we found that none of the three selected site sID  $\beta$ II fragments, F04, F36, and F41, are cytotoxic under the experimental conditions used (i.e., up to a fragment concentration of 200  $\mu$ M; Figure S4). To test whether linking a bulky group to the



**Scheme 1.** Reaction conditions for Hantzsch synthesis (**3–5**, **8–10** and **14–22**), reductive amination (**1**, **2**), and amide derivatives (**11–13**). *Reagents and conditions:* (i) 4-acetamidophenacyl bromide (1 equiv), thiourea (1.1 equiv), EtOH, 1 h, reflux, yield 27–96%; (ii) N-(4-(2-aminothiazol-4-yl)phenyl)acetamide (1 equiv), aldehyde (2 equiv), AcOH (5 equiv), NaBH(OAc)<sub>3</sub> (2.8 equiv), DCE, 48 h, rt, yield 24–56% (iii) 2-bromo-1-(4-nitrophenyl)ethanone (1 equiv) and N-(3-fluorophenyl)thiourea (1.1 equiv), EtOH, 1 h, reflux, yield 72%; (iv) Fe (15 equiv), 24.5% HCl (2 equiv), iPrOH, 1 h, 60°C, yield 36%; (v) acyl chloride (1.1 equiv), DIPEA (2 equiv), DCM, 30 min, 0°C, 1–2 h, rt, yield 52–71%.



**Scheme 2.** Reaction conditions for the synthesis of compounds **6** and **7**. *Reagents and conditions:* (i) N-(4-(2-aminothiazol-4-yl)phenyl)acetamide (1 equiv), benzoylchloride (2 equiv), triethylamine (2 equiv), anhydrous DCM, 0 °C to rt, N<sub>2</sub>, 16 hours, yield 25%; (ii) N-(4-(2-aminothiazol-4-yl)phenyl)acetamide (1 equiv), 2-methanesulfonyl chloride (1 equiv), anhydrous DCM, pyridine, 0 °C to rt, N<sub>2</sub>, 6 hours, yield 70%.

thiazoleamine moiety of F04 produces an active compound, we synthesized a first set of derivatives (Table 1). The rationale was to determine which bulky group and which linker length is suited to exploit the deep hydrophobic cavity of  $\alpha$ -tubulin as suggested by fragments F36 and F41 (Figure 1B–D). To this end, we attached either an aromatic phenyl (**4**), an aliphatic cyclohexyl (**3**), an aliphatic isobutyl (**1**), an aliphatic neopentyl (**2**), or a polar methanesulfonyl (**7**) to the thiazoleamine moiety of F04. To test the importance of the length of the linker between the amine and the introduced phenyl group, we elongated the linker by one carbon atom (**5**) or replaced the amine linker with an amide (**6**) in the phenyl derivative **4**.

The activities of the derivatives were assessed using cytotoxicity assays. As summarized in Table 1 and shown in Figure S4, **4** displayed a well measurable effect on HeLa cells with an IC<sub>50</sub> of 48  $\mu$ M (95 % confidence interval: 47–50  $\mu$ M), while **3** and **2** showed IC<sub>50</sub> values of >80  $\mu$ M; the remaining derivatives **6**, **1**, **5**, and **7** were not cytotoxic under the conditions used. These results suggest that our fragment linking strategy already produces an active compound and

that neither a longer linker nor an aliphatic or polar modification is beneficial to gain potency.

To verify our design, we solved the crystal structure of the phenyl derivative **4** in complex with a well-established tubulin crystal system composed of two longitudinally aligned  $\alpha\beta$ -tubulin heterodimers (the tubulin monomers are denoted  $\alpha$ Tub1,  $\beta$ Tub1,  $\alpha$ Tub2, and  $\beta$ Tub2), one copy of the stathmin-like protein RB3, and one copy of tubulin tyrosine ligase (the complex is denoted T<sub>2</sub>R-TTL;<sup>[10]</sup>) to high resolution (Table S1; Figure S5A). The tubulin-**4** complex structure revealed that the derivative indeed targeted site sID  $\beta$ II (Figure 2A). In agreement with our structural considerations (see above), we observed that this modification indeed abolished binding of **4** to the second binding site sID  $\beta$ III of  $\beta$ -tubulin in our crystal system (Figure S3D).

We further found that the acetanilide motif of **4**, which interacts with residues  $\alpha$ T257,  $\beta$ N102, and  $\beta$ W407 displays the same tubulin-binding mode as F04 (Figure 2A). Accordingly, the introduced phenyl moiety is inserted into the deep hydrophobic cavity of  $\alpha$ -tubulin similar to the fragment F41 binding pose, and by doing so, displaced the three structural

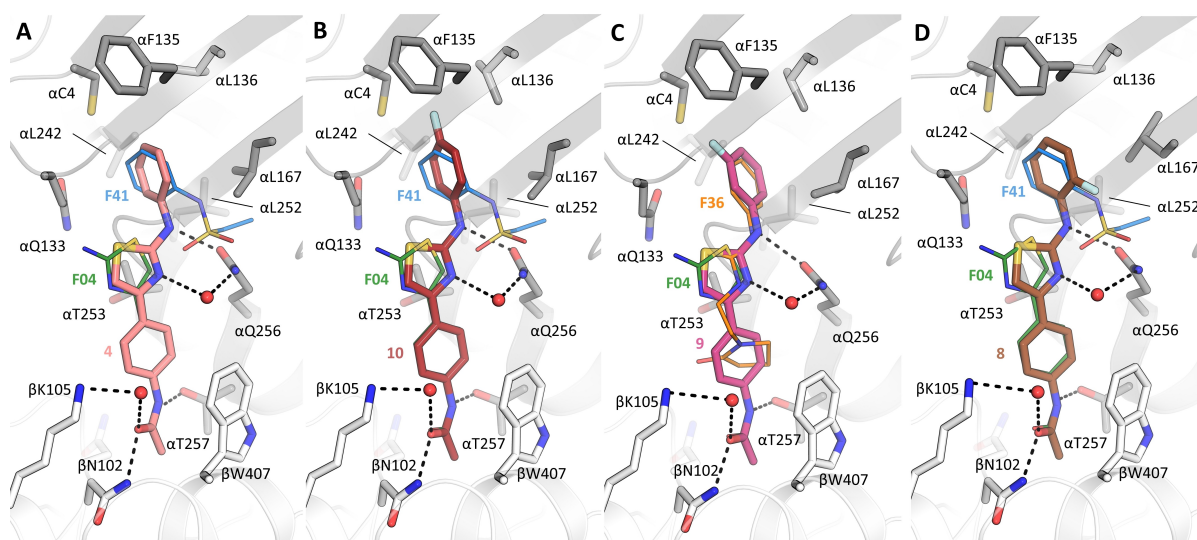


**Figure 2.** Structural basis of **4** and its meta-, ortho-, and para-fluorinated derivatives. A) Superimposition of the binding site of the tubulin-**4** complex structure onto the ones of tubulin-F04 (green) and tubulin-F41 (blue). B) Superimposition of the binding site of the tubulin-**10** complex structure onto the ones of tubulin-F04 (green) and tubulin-F41 (blue). C) Superimposition of the binding site of the tubulin-**9** complex structure onto the ones of tubulin-F04 (green) and tubulin-F36 (orange). D) Superimposition of the binding site of the tubulin-**8** complex structure onto the ones of tubulin-F04 (green) and tubulin-F41 (blue). The  $\alpha$ - and  $\beta$ -tubulin monomers are shown in gray and white ribbon representation, respectively. Residues forming the binding site are shown in stick representation and are labeled in black. The same atom color scheme as in Figure 1B has been used. Hydrogen bonds are shown as dashed black lines.

**Table 1:** Cell cytotoxicity IC<sub>50</sub> values.

Cpd#	R <sup>1</sup>	R <sup>2</sup>	IC <sub>50</sub> <sup>[a]</sup> [μM]	Cpd#	R <sup>1</sup>	R <sup>2</sup>	IC <sub>50</sub> <sup>[a]</sup> [μM]
F04	H	CH <sub>3</sub>	n/a	12			34 (31–36)
1		CH <sub>3</sub>	n/a	13			38 (33–40)
2		CH <sub>3</sub>	> 80 <sup>[b]</sup>	14		CH <sub>3</sub>	59 (53–65)
3		CH <sub>3</sub>	> 80 <sup>[b]</sup>	15		CH <sub>3</sub>	37 (33–40)
4		CH <sub>3</sub>	48 (47–50)	16		CH <sub>3</sub>	39 (34–45)
5		CH <sub>3</sub>	n/a	17		CH <sub>3</sub>	71 (64–78)
6		CH <sub>3</sub>	n/a	18		CH <sub>3</sub>	8.8 (8.1–9.5)
7		CH <sub>3</sub>	n/a	19		CH <sub>3</sub>	n/a
8		CH <sub>3</sub>	> 80 <sup>[b]</sup>	20		CH <sub>3</sub>	19 (18–21)
9		CH <sub>3</sub>	30 (26–33)	21		CH <sub>3</sub>	50 (47–54)
10		CH <sub>3</sub>	> 80 <sup>[b]</sup>	22		CH <sub>3</sub>	43 (40–47)
11			38 (37–41)				

[a] HeLa cells were used for performing the assays. The 95 % confidence interval is given in brackets. [b] A clear effect on cells was observed but the data could not be fitted. Cpd#, compound number. n/a, no effect observed on cells under the experimental conditions tested. The dose-response curves of all experiments are shown in Figure S4.

water molecules seen in the tubulin-F04 complex structure. However, to achieve this specific orientation, the thiazole

heterocycle of **4** had to flip by approximately 180° compared to the one of F04. This conformational change allowed **4** to

establish two new hydrogen bonds between its amine and its thiazole-nitrogen with the side chain of  $\alpha$ Q256; latter interaction is water mediated.

### Further optimization

The crystal structure of the tubulin-**4** complex revealed that additional space in the tubulin-binding pocket is available for extending both the phenyl and the acetyl groups of the ligand. Notably, fragment F41 contains a polar fluorine on its phenyl group (Figure 1BC). In the following, we thus tested the effect of attaching different substituents to the phenyl ring of **4** (Table 1). To select for the most promising substituents for subsequent chemical synthesis, chemical modifications were guided by visual inspection of the tubulin-**4** complex structure, by docking studies, and by molecular mechanics with generalized Born and surface area solvation (MM/GBSA) calculations (Table S2).

In a first step, we assessed whether attaching a fluorine atom to either the ortho- (**8**), meta- (**9**), or para-position (**10**) of the phenyl ring of **4** has an effect on the activity of the compound. As summarized in Table 1 and shown in Figure S4, the ortho- or para-position substitutions resulted in a significantly reduced cytotoxic activity of the derivatives with  $IC_{50}$  values of  $>80\text{ }\mu\text{M}$  compared to the parent compound. In contrast, the meta-position substitution resulted in an improved potency with an  $IC_{50}$  value of  $30\text{ }\mu\text{M}$  (95 % confidence interval:  $26\text{--}33\text{ }\mu\text{M}$ ). We also tested the effect of modifications of the acetyl functional group of **4** by elongating it with an ethyl (**11**), isopropyl (**12**), or cyclopropyl (**13**) substituent. These modifications did not result in a significantly improved activity (Table 1; Figure S4); this strategy was thus not followed any further.

We sought to reinforce our findings on the gain in activity of **4** upon introducing modifications at the meta-position of its phenyl group. To this end, we synthesized two additional series of compounds with either a methyl group (**14**, **15**, and **16**) or trifluoromethyl substituents (**17**, **18**, and **19**) in the ortho-, meta-, or para-position (Table 1). Cytotoxicity assays revealed that the two types of modifications at the ortho-position retained some compound activity with  $IC_{50}$  values of  $59\text{ }\mu\text{M}$  (95 % confidence interval:  $53\text{--}65\text{ }\mu\text{M}$ ) and  $71\text{ }\mu\text{M}$  (95 % confidence interval:  $64\text{--}78\text{ }\mu\text{M}$ ; Table 1; Figure S4). In the case of the para-substitutions, the methyl group resulted in a slightly improved  $IC_{50}$  of  $39\text{ }\mu\text{M}$  (95 % confidence interval:  $34\text{--}45\text{ }\mu\text{M}$ ) over the parent compound, while attaching a trifluoromethyl group at this position abrogated activity. As with the fluorine derivatives, the best results were attained with the meta-substituted compounds with the one containing the trifluoromethyl group displaying the so far lowest  $IC_{50}$  value of  $8.8\text{ }\mu\text{M}$  (95 % confidence interval:  $8.1\text{--}9.5\text{ }\mu\text{M}$ ; Table 1; Figure S4).

Together, these results demonstrate that modification of the phenyl meta-position of **4** is the best strategy to gain potency. To test whether other substitutions could further increase potency, we synthesized three additional derivatives of **4** in which either a *m*-chloro (**20**), a *m*-hydroxyl (**21**), or a *m*-methoxy (**22**) group was introduced in its phenyl ring.

However, none of these derivatives was more active than the trifluoromethylated compound **18** (Table 1; Figure S4).

### Structural Characterization of Fluorinated Derivatives

To provide a structural explanation for the preference of meta- over ortho- and para-position substitutions of the phenyl ring of **4**, we solved the crystal structures of the three single fluorinated derivatives **10**, **9**, and **8** in complex with tubulin (Table S1; Figure S5B–D). While none of the modifications influenced the interaction network formed between the core of **4** and tubulin (Figure 2A), one major difference was the orientation of the *m*-fluorophenyl group in its binding pocket. While the ortho- and para-substituted phenyl groups were oriented similar to the ones of the parent compound and fragment F41 (Figure 2BD), the one of the meta-substituted derivative was oriented in an almost identical way as the phenyl group of fragment F36 (Figure 2C).

When compared to the tubulin-**4** complex structure, we further observed slight conformational changes of the side chains of the  $\alpha$ -tubulin residues  $\alpha$ L136 and  $\alpha$ L167 upon ligand binding, which allow accommodating the respective fluorine atom at the different phenyl positions of the derivatives. The presence of fluorine at the para-position of the phenyl causes the  $\delta$ 1-methyl group of the side chain of  $\alpha$ L136 to move upward compared to its conformation in the tubulin-**4** complex structure while keeping the phenyl in the same orientation (Figure S6A–D). In this context, the hydrophobic environment around the phenyl para-position may explain why attaching a hydrophobic methyl group at this position displays a higher activity. Conversely, the presence of a slightly bulkier trifluoromethyl group at the same position can reduce the activity of the compound due to steric hindrance (Figure S6B). Polarization effects might also play a role since the hydrogens of a methyl are partially positively charged whereas fluorine atoms of a trifluoromethyl group bear partial negative charges. In the case of the *o*-fluorophenyl derivative, the substituent causes a displacement of the  $C\gamma$  atom of the  $\alpha$ L167 side chain by  $1.8\text{ }\text{\AA}$  similar to what is also seen in the tubulin-F41 complex structure (Figure 2D; Figure S6G). Furthermore, due to the large open space surrounding the ortho-position of the benzene, possible substituents should be carefully designed to engage in favorable interactions with residues forming the pocket (Figure S6H).

Notably, the upward facing conformation of the  $\alpha$ L136 side chain is also observed in the tubulin structure in complex with the *m*-fluorophenyl derivative. However, in this case the conformational change is due to the different orientation of the benzene ring compared to the one seen for the ortho- and para-substituted derivatives (Figure S6CEG). Notably, the fluorine atom of the meta-substituted derivative interacts favorably with a small pocket formed by the side chains of  $\alpha$ C4 and  $\alpha$ Q133, and the main chains of  $\alpha$ Q133 and  $\alpha$ F135 (Figure S6EF).

To provide a structural explanation of why a trifluoromethyl substituent attached to the meta-position of

the phenyl group of the parent compound produces the most active derivative, we solved the crystal structure of **18** in complex with tubulin (Table S1; Figure S5E). Interestingly, the structure revealed that while the binding mode including the hydrogen-bonding network of **18** is essentially the same as for the *m*-fluorophenyl derivative **9**, its *m*-trifluoromethyl group points in the opposite direction compared to the single fluorine substituted derivative (Figure 3A). This change in orientation may explain the improved activity of **18** over **9**, as the trifluoromethyl group is now deeply inserted into a hydrophobic pocket formed by the side chains of residues  $\alpha$ C4,  $\alpha$ F52,  $\alpha$ L136,  $\alpha$ L167,  $\alpha$ L242, and  $\alpha$ L252 (Figure 3AB). This is in contrast to the derivative with the single *m*-fluorine that rather weakly interacts with the side chains of residues  $\alpha$ C4 and  $\alpha$ Q133, and the main chains of  $\alpha$ Q133 and  $\alpha$ F135 (Figure 2C).

Together, these results and considerations indicate that the precise conformations of the *m*-trifluoromethyl substituted phenyl ring of **18** and of the  $\alpha$ L136 and  $\alpha$ L167 residue side chains, in combination with optimal packing interactions between the trifluoromethyl moiety and a hydrophobic pocket in  $\alpha$ -tubulin is most likely responsible for the activity of the compound in the low micromolar range. From here onwards, we refer to **18** as “Todalam” and to its binding site as the “Todalam site”.

#### Effect of Todalam on Tubulin and Microtubules In Vitro and In Cells

Next, we characterized the molecular mechanism of action of Todalam on tubulin and microtubules. As a first step, we

sought to test whether the observed cytotoxicity of Todalam is indeed linked to an effect on tubulin and microtubules. First, we used a standard in vitro tubulin polymerization assay in which we incubated 30  $\mu$ M of tubulin with increasing amounts of Todalam between 0 and 1000  $\mu$ M under polymerizing conditions. As shown in Figure 4A and Figure S7A, Todalam had already an effect on tubulin polymerization at stoichiometric concentrations and fully inhibited microtubule formation at a concentration of 100  $\mu$ M with an  $IC_{50}$  of  $48 \pm 17$   $\mu$ M. Inspection of tubulin samples (20  $\mu$ M), which were incubated under depolymerizing conditions with 150  $\mu$ M of Todalam by negative staining transmission electron microscopy showed the formation of ring-like tubulin oligomers (Figure 4B). Similar ring-like tubulin oligomers are also observed by incubating tubulin with the interdimer-interface binding and microtubule-destabilizing agent vinblastine (Figure S7B).<sup>[13]</sup>

To test the effect of Todalam on microtubules in different cell types, we performed immunostaining assays. The representative fluorescence confocal microscopy images shown in Figures 5A and S7C reveal that disruption of the microtubule network in HMF3a, MDAMB 231, and HeLa cells is achieved after 4 hours of incubation with 20  $\mu$ M of the compound. Consequently, the shape of both the cells themselves and their nuclei changed dramatically and the cells lost the capability to stay attached to the cover slips. As shown in Figure 5B for HMF3a cells, this phenotype could be largely reverted after washing out the compound and let the cells recover for 16 hours. We further performed a cell cycle analysis with HMF3a cells after treatment with 20  $\mu$ M Todalam for 24 hours using flow cytometry and found that

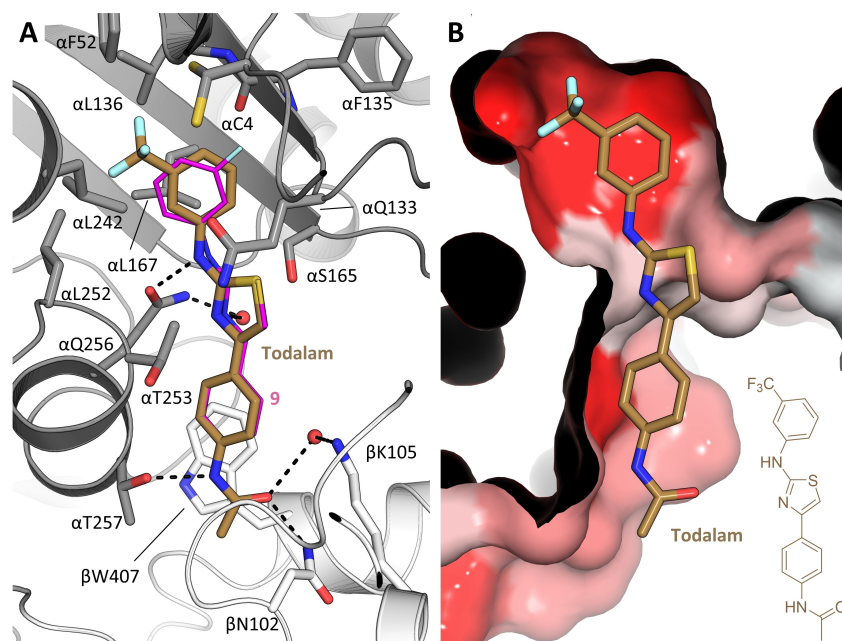


**Figure 3.** Structural basis of Todalam. A) Binding mode of Todalam as seen in the crystal structure of the tubulin-Todalam complex superimposed onto the one of the tubulin-**9** complex. The  $\alpha$ - and  $\beta$ -tubulin monomers are shown in gray and white ribbon representation, respectively. Residues forming the binding site are shown in stick representation and are labeled in black. The same atom color scheme as in Figure 1B has been used. Hydrogen bonds are shown as dashed black lines. B) The Todalam site is shown in surface representation and colored with a gradient from red for a hydrophobic to white for a hydrophilic environment. The chemical structure of Todalam is shown on the bottom right of the panel.

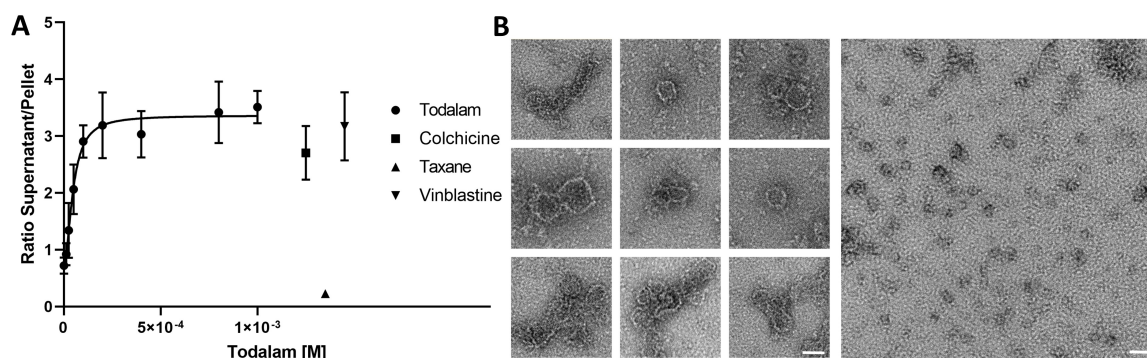


**Figure 4.** Effect of Todalam on tubulin and microtubules in vitro. A) Inhibition of tubulin polymerization assessed by microtubule pelleting assays performed in the presence of the indicated increasing amounts of Todalam or control compounds at 10  $\mu$ M. Tubulin concentration: 30  $\mu$ M. For raw data, see Figure S7A. B) Negative staining electron micrographs of tubulin incubated together with 150  $\mu$ M Todalam (gallery) or without the compound (overview micrograph). Tubulin concentration: 20  $\mu$ M. Scale bars, 50 nm.

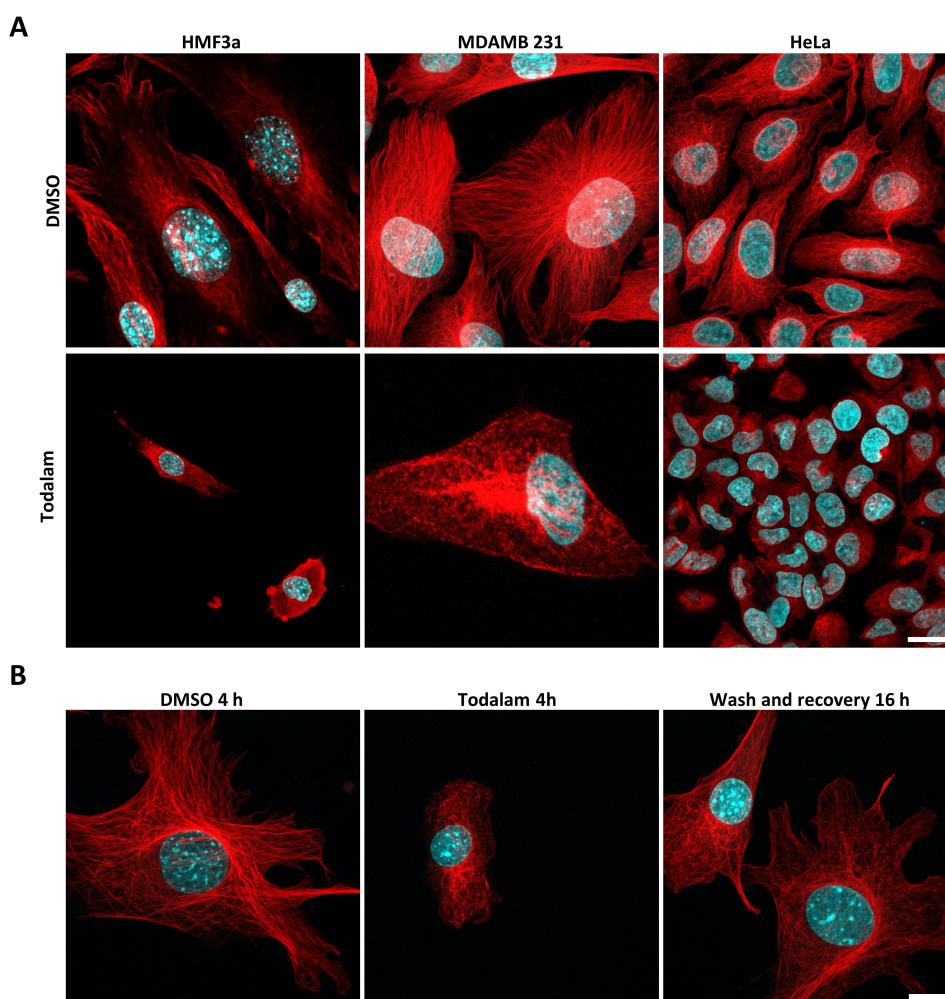


**Figure 5.** Effect of Todalam on microtubules in cells. A) Representative fluorescence confocal microscopy images of HMF3a, MDAMB 231, and HeLa cells that were treated either with 0.5% DMSO (control, upper panels) or 20  $\mu$ M Todalam (lower panels) for 4 hours. Microtubules are immunostained with an anti  $\alpha$ -tubulin antibody and are colored in red; the cell nuclei are stained with DAPI (4',6-diamidin-2-phenylindole) and are colored in blue. B) Drug wash out experiments. Representative confocal images of HMF3a cells that were treated with 20  $\mu$ M Todalam for 4 hours, subsequently washed with culture media, and left to recover for 16 hours. The immunostaining assay is identical to the one shown in panel A. Scale bars, 20  $\mu$ m.

the compound induced a 2–3 fold increase in the G2 cell population compared to the DMSO control (Figure S7D). Together, these results are consistent with Totolam acting as a reversible microtubule-destabilizing agent in vitro and in cells.

### Molecular Mechanism of Action of Totolam

How does Totolam destabilize microtubules? To answer this question, we analyzed Totolam binding to tubulin in the context of a microtubule. It is well established that the  $\alpha\beta$ -tubulin heterodimer undergoes a “curved-to-straight” conformational change upon incorporation into the microtubule lattice. This global conformational change is brought about by a rotational movement of the intermediate domain of both the  $\alpha$ - and  $\beta$ -tubulin monomers with respect to their N- and C-terminal domains.<sup>[14]</sup> Notably, the  $\alpha$ -tubulin half site of the Totolam pocket is formed by secondary structure elements stemming from both the N-terminal ( $\alpha$ S4 and  $\alpha$ S5) and intermediate ( $\alpha$ H8) domains of  $\alpha$ -tubulin. As shown in Figure 6A, helix  $\alpha$ H8 moves towards strands  $\alpha$ S4 and  $\alpha$ S5 when the  $\alpha$ -tubulin monomer transitions from the curved to the straight conformation. In the presence of Totolam, however, this movement causes helix  $\alpha$ H8 to clash into the core moiety of the compound. Thus, Totolam seems to act as a “steric molecular plug” that hinders helix  $\alpha$ H8 to move closer to strands  $\alpha$ S4 and  $\alpha$ S5 during the curved-to-straight tubulin dimer conformational transition.

The situation is different on the  $\beta$ -tubulin half site of the Totolam pocket, which is formed by secondary structure elements from the N-terminal ( $\beta$ T3) and the C-terminal domain ( $\beta$ H11'). Since both  $\beta$ -tubulin domains move in accord during the curved-to-straight tubulin dimer conformational change, the conformation of this Totolam half site is maintained; the ligand is thus expected to bind to both  $\beta$ -tubulin conformational states (Figure 6B).

Due to its particular binding site located between two longitudinally aligned tubulin dimers, Totolam can bind simultaneously both the  $\alpha$ - and  $\beta$ -tubulin monomers of two tubulin dimers (Figures 1A and 3). This readily explains the promotion of tubulin ring-like oligomer formation in the presence of Totolam in vitro (Figure 4B). Notably, vinblastine also destabilizes microtubules by promoting ring-like oligomers though by binding to a different composite site formed between two longitudinally aligned tubulin dimers.<sup>[15]</sup> To test whether Totolam and vinblastine can bind to tubulin simultaneously, we soaked T<sub>2</sub>R-TTL crystals with both compounds and solved the complex structure by X-ray crystallography. As expected, we found that both ligands bound to two different sites located at the tubulin interdimer interface in the T<sub>2</sub>R-TTL complex (Figure S8A). We also tested if Totolam and vinblastine when applied together can augment their cell growth inhibitory effects. We found that when reciprocally assessed and using a low concentration of one of the compounds, which does not affect cell proliferation (Figure S8B), the compounds acted synergistically (Figure S8CD).

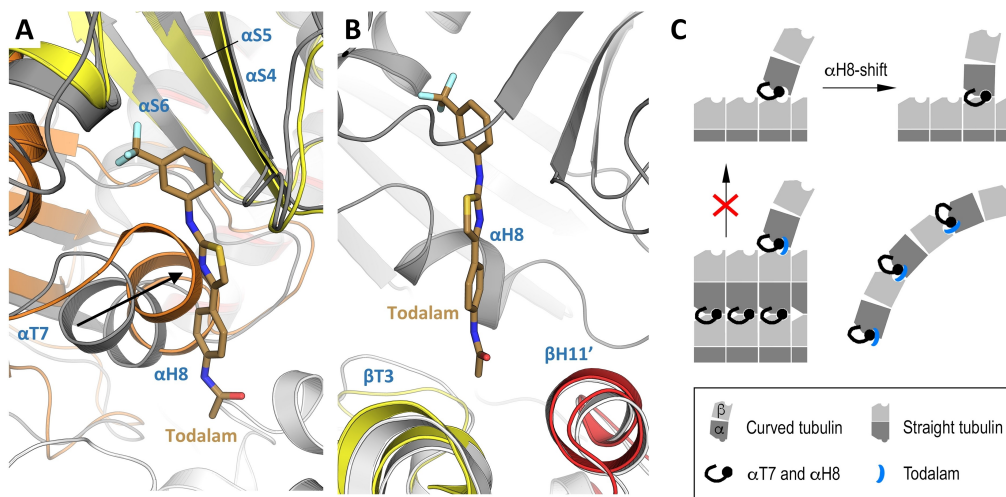


**Figure 6.** Molecular mechanism of action of Totolam. A, B) Superimposition of the  $\alpha$ -tubulin (A) and  $\beta$ -tubulin (B) half sites of the Totolam pocket in the curved and straight conformation of the tubulin dimer. The curved conformational states of the  $\alpha$ - and  $\beta$ -tubulin subunits are shown in grey and white ribbon representation, respectively. The straight states of tubulin monomer structures were taken from PDB ID 6DPV and are colored according to their three domains: N-terminal domain in yellow (residues 1–205), intermediate domain in orange (residues 206–384), and C-terminal domain in red (residues 385–440). For the superposition of the curved and straight conformational states of  $\alpha$ - and  $\beta$ -tubulin, the central strands  $\alpha$ S1,  $\alpha$ S2,  $\alpha$ S4,  $\alpha$ S5, and  $\alpha$ S6, or  $\beta$ S1,  $\beta$ S2,  $\beta$ S4,  $\beta$ S5, and  $\beta$ S6 were used, respectively. Secondary structure elements are labelled in blue. For simplicity, strand  $\alpha$ S1 that is not involved in the molecular mechanism of action of Totolam was removed in panel A. The black arrow in panel A indicates the movement of helix  $\alpha$ H8 during the curved-to-straight conformational transition of the tubulin dimer. C) Schematic illustration of the molecular mechanism of action of Totolam on tubulin and microtubules. Upper panel: Tubulin assembly in the absence of Totolam, highlighting the shift of the  $\alpha$ H8 helix of  $\alpha$ -tubulin required for proper accommodation of the incoming tubulin dimer. Lower Panel: The presence of Totolam blocks the shift of the  $\alpha$ H8 helix, thereby preventing microtubule growth and promoting the formation of ring-like oligomers.

Together, these observations suggest that Todalam destabilized microtubules via predominantly two mechanisms (Figure 6C): (i) by acting as a steric molecular plug that inhibits the curved-to-straight conformational activation switch in  $\alpha$ -tubulin, and (ii) by locking tubulin dimers into microtubule-assembly incompetent oligomers. Our results further indicate that Todalam and vinblastine in combination can act synergistically to inhibit cell growth.

## Conclusion

Here, we capitalized on our previously performed crystallographic fragment screen<sup>[11]</sup> and generated the antitubulin compound Todalam using a structure-based drug-discovery approach. We demonstrate that Todalam binds to a novel site in tubulin, which we dubbed the Todalam site. We further show that Todalam kills different type of mammalian cells, induces G2/M arrest, disrupts cellular microtubule networks, and can inhibit cell growth in a synergistic manner in combination with vinblastine. Todalam achieves its effect by locking  $\alpha$ -tubulin in an inactive conformational state and by sequestering tubulin dimers. To the best of our knowledge, Todalam is the first-ever, fully rationally designed tubulin inhibitor with an original molecular mechanism of action.

Crystallography-based fragment screening is a very powerful approach for hit discovery, which has already lead to several drugs and chemical probes.<sup>[16]</sup> A key question in the field is, however, whether the fragments identified in this manner are useful starting points for the rapid development of lead-like molecules.<sup>[17]</sup> Our study highlights that this is indeed the case for the complex anticancer target tubulin. We generated a limited number of compounds with only two rounds of straightforward chemical synthesis guided by structural and computational analyses, which led to a lead-like, small molecule tubulin inhibitor with a molecular weight of 377 Da. The Todalam scaffold sets an excellent basis for a deeper SAR exploration. In this context, we noted that an *m*-chloro substitution of the parent compound's phenyl group displayed a favorable IC<sub>50</sub>. We thus anticipate that additional modifications of the core part of Todalam in combination with the further exploration of its acetanilide moiety should improve the activity of Todalam down to the low nanomolar range.

Our series of compounds bear a good chemical tractability. This remarkably contrasts with approved antitubulin drugs used in the clinic, which are typically derived from natural products and display complex chemical structures with multiple chiral centers and complicated synthetic routes - their total synthesis and chemical modification is thus not straightforward. In contrast, we here show that a rational approach, along with a limited straightforward SAR exploration, is also possible for tubulin inhibitors, providing unique opportunities to overcome some of the bottlenecks associated with drug discovery programs targeting tubulin.

Taken together, our results demonstrate the usefulness of tubulin-binding fragments as valuable starting points for innovative antitubulin drug and chemical probe discovery

campaigns. They further highlight that crystallographic fragment screening is particularly powerful with complex targets for which only natural compounds have so far reached clinical practice.

## Author Contributions

T.M. designed the research, performed crystallography, biochemistry and cell biology work, analyzed the data, prepared figures, wrote the first draft of the manuscript. L.M. designed the research, performed chemistry and computational work, analyzed the data. J.A.O. designed the research, supervised the chemistry work, analyzed the data. T.B.B. prepared negatively stained grids, recorded transmission electron microscopy images. D.G. performed computational work. B.R. performed cell immunostaining and cell cycle analysis work. A.E.P. designed the research, performed and supervised the crystallography work, analyzed the data. A.C. designed the research, supervised the chemistry and computational work, analyzed the data. M.O.S. designed the research, supervised the crystallography, biochemistry and cell biology work, analyzed the data, wrote the paper with input from all authors, coordinated the project.

## Acknowledgements

We are indebted to Todorov Tihomir for the help with the flow cytometry experiments and to Prof G.V. Shivashankar for the support with the cell assays. We thank the BioEM Lab of the Biozentrum, University of Basel, Switzerland, for their support and use of the electron microscope. X-ray diffraction data were collected at the beamline X06DA at the Swiss Light Source (Paul Scherrer Institut, Villigen PSI, Switzerland). This work has been supported by grants from the Regione Lombardia (ID 239047 NEON; to A.C.) and from the Swiss National Science Foundation (31003A\_166608 and 310030\_192566; to M.O.S.). Open access funding provided by ETH-Bereich Forschungsanstalten.

## Conflict of Interest

The authors declare no conflict of interest.

## Data Availability Statement

Coordinates of the X-ray crystal structures have been deposited in the RCSB PDB (www.rcsb.org): Tubulin-4: 5SB3; Tubulin-8: 5SB4; Tubulin-9: 5SB5; Tubulin-10: 5SB6; Tubulin-Todalam: 5SB7; Tubulin-Todalam-vinblastine: 7Z7D. The data that support the findings of this study are available from the corresponding author upon reasonable request.

**Keywords:** Fragments • Microtubule-Targeting Agents • Molecular Mechanism of Action • Rational Drug Design • Tubulin

- [1] a) C. H. Yang, S. B. Horwitz, *Int. J. Mol. Sci.* **2017**, *18*, 1733; b) N. C. Miltenburg, W. Boogerd, *Cancer Treat. Rev.* **2014**, *40*, 872–882; c) M. Kavallaris, *Nat. Rev. Cancer* **2010**, *10*, 194–204.
- [2] a) W. H. Xiao, H. Zheng, G. J. Bennett, *Neuroscience* **2012**, *203*, 194–206; b) S. Sobue, N. Mizutani, Y. Aoyama, Y. Kawamoto, M. Suzuki, Y. Nozawa, M. Ichihara, T. Murate, *Biochem. Biophys. Res. Commun.* **2016**, *479*, 808–813; c) J. P. Guastalla III, V. Diéras, *Br. J. Cancer* **2003**, *89*, S16–S22.
- [3] a) N. E. LaPointe, G. Morfini, S. T. Brady, S. C. Feinstein, L. Wilson, M. A. Jordan, *Neurotoxicology* **2013**, *37*, 231–239; b) T. Nakata, H. Yorifuji, *Neurosci. Res.* **1999**, *35*, 113–122; c) C. Theiss, K. Meller, *Cell Tissue Res.* **2000**, *299*, 213–224.
- [4] P. W. Baas, F. J. Ahmad, *Brain* **2013**, *136*, 2937–2951.
- [5] a) N. Gaillard, A. Sharma, I. Abbaali, T. Liu, F. Shilliday, A. D. Cook, V. Ehrhard, M. Bangera, A. J. Roberts, C. A. Moores, N. Morrisette, M. O. Steinmetz, *EMBO Mol. Med.* **2021**, *13*, e13818; b) E. Soleilhac, L. Brillet-Guéguen, V. Roussel, R. Prudent, B. Touquet, S. Dass, S. Aci-Sèche, V. Kasam, C. Barette, A. Imbert, V. Breton, M. Vantard, D. Horvath, C. Botté, I. Tardieux, S. Roy, E. Maréchal, L. Lafanechère, *Int. J. Mol. Sci.* **2018**, *19*, 3085.
- [6] a) B. P. Chatterji, B. Jindal, S. Srivastava, D. Panda, *Expert Opin. Ther. Pat.* **2011**, *21*, 167–186; b) B. Fennell, J. Naughton, J. Barlow, G. Brennan, I. Fairweather, E. Hoey, N. McFerran, A. Trudgett, A. Bell, *Expert Opin. Drug Discovery* **2008**, *3*, 501–518.
- [7] <http://www.clinicaltrials.gov>.
- [8] M. O. Steinmetz, A. E. Prota, *Trends Cell Biol.* **2018**, *28*, 776–792.
- [9] S. Matthew, Q. Y. Chen, R. Ratnayake, C. S. Fermaintt, D. Lucena-Agell, F. Bonato, A. E. Prota, S. T. Lim, X. Wang, J. F. Díaz, A. L. Risinger, V. J. Paul, M. Oliva, H. Luesch, *Proc. Natl. Acad. Sci. USA* **2021**, *118*, e2021847118.
- [10] a) A. E. Prota, K. Bargsten, D. Zurwerra, J. J. Field, J. F. Diaz, K. H. Altmann, M. O. Steinmetz, *Science* **2013**, *339*, 587–590; b) A. E. Prota, M. M. Magiera, M. Kuijpers, K. Bargsten, D. Frey, M. Wieser, R. Jaussi, C. C. Hoogenraad, R. A. Kammerer, C. Janke, M. O. Steinmetz, *J. Cell Biol.* **2013**, *200*, 259–270.
- [11] T. Mühlethaler, D. Gioia, A. E. Prota, M. E. Sharpe, A. Cavalli, M. O. Steinmetz, *Angew. Chem. Int. Ed.* **2021**, *60*, 13331–13342; *Angew. Chem.* **2021**, *133*, 13443–13454.
- [12] J. Löwe, H. Li, K. H. Downing, E. Nogales, *J. Mol. Biol.* **2001**, *313*, 1045–1057.
- [13] A. E. Prota, F. Danel, F. Bachmann, K. Bargsten, R. M. Buey, J. Pohlmann, S. Reinelt, H. Lane, M. O. Steinmetz, *J. Mol. Biol.* **2014**, *426*, 1848–1860.
- [14] R. B. Ravelli, B. Gigant, P. A. Curmi, I. Jourdain, S. Lachkar, A. Sobel, M. Knossow, *Nature* **2004**, *428*, 198–202.
- [15] B. Gigant, C. Wang, R. B. Ravelli, F. Roussi, M. O. Steinmetz, P. A. Curmi, A. Sobel, M. Knossow, *Nature* **2005**, *435*, 519–522.
- [16] a) D. A. Erlanson, S. W. Fesik, R. E. Hubbard, W. Jahnke, H. Jhoti, *Nat. Rev. Drug Discovery* **2016**, *15*, 605–619; b) practical-lfragments.blogspot.com.
- [17] T. Krojer, J. S. Fraser, F. von Delft, *Curr. Opin. Struct. Biol.* **2020**, *65*, 209–216.

Manuscript received: March 21, 2022

Accepted manuscript online: April 11, 2022

Version of record online: April 25, 2022